

Cite this: DOI: 10.1000/xxxxxx

Self-assembly of active bivalent Brownian particles [†]

Caterina Landi ^a, John Russo ^b, Francesco Sciortino ^b, Chantal Valeriani ^a

Pre-proof
Accepted Date

DOI: 10.1000/xxxxxx

In the present work, with the intent of exploring the out-of-equilibrium polymerization of active patchy particles in linear chains, we study a suspension of active bivalent Brownian particles (ABBP). At all studied temperatures and densities, ABBP self-assemble in aggregating chains, as opposed to the uniformly space-distributed chains observed in the corresponding passive systems. The main effect of activity, other than inducing chain aggregation, is to reduce the chain length and favour alignment of the propulsion vectors in the bonding process. At low activities, attraction dominates over activity in the bonding process, leading self-assembly to occur randomly regardless of the particle orientations. Interestingly, we find that at the lowest temperature, as density increases, chains aggregate forming a novel state: MISP, i.e., Motility-Induced Spirals, where spirals are characterised by a finite angular velocity. On the contrary, at the highest temperature, density and activity, chains aggregate forming a different novel state (a spinning crystalline cluster) characterised by a compact and hexagonal ordered structure, both translating and rotating. The rotation arises from an effective torque generated by the presence of competing domains where particles self-propel in the same direction.

1 Introduction

In the last decades, significant progress has been made in understanding the structural and dynamical properties of liquids through the investigation of colloidal particles interacting via spherically symmetric or (more realistic) anisotropic forces¹. A practical model proposed to study anisotropic interactions between colloidal particles is the so-called “patchy particle” model, consisting on hard-spheres whose surface is decorated with a finite number of short-range attractive sites^{2,3}. Patchy particles have allowed to elucidate the behavior of network-forming materials^{4,5}, such as water⁶ or silica⁷, finite aggregates, such as surfactant micelles⁸, or more complex structures, such as proteins^{9,10}. Patchy particles also represent a novel class of building blocks for constructing precise structure, where the arrangements and the selectivity of the sites dictate the overall structure of the assemblies^{11–14}. Indeed, the bottom-up approach of patchy colloidal self-assembly has proven pivotal for technological advancements across diverse fields, including materials science¹⁵, pharmaceutical industry¹⁶, electronics¹⁷, nanotechnology¹⁸, and even food technology¹⁹.

Optimization of colloidal self-assembly, inspired by biological matter, has been further obtained by introducing activity²⁰ on simple colloids, with possible applications ranging from the targeted drug delivery²¹ to the autonomous depollution of contaminated water and soils²². Nevertheless, so far, the majority of the published work on active colloidal matter has focused on sus-

pensions of active particles interacting via an isotropic potential (attractive²³ or repulsive²⁴). Only more recently, the field of active matter has branched out to explore the interplay between activity and anisotropic interactions, with the goal of developing a systematic understanding of how active forces can be exploited together with anisotropic forces to design assemblies with desired structural and functional features^{25–27}. Full control on the the complex dynamics of active patchy colloids remains yet challenging. So far, research has been performed into tuning the shape, size and composition of the patches in order to control autonomous locomotion and spontaneous assembly^{27–29}. Specific interactions can be obtained by implementing lock and key groups on the particles’ surface, such as DNA oligonucleotides, protein cross-linkers or antibody-antigen binding pairs³⁰. Due to their ability to self-assemble into chains, sheets, rings, icosahedra, tetrahedra, etc., patchy colloids provide access to a broad range of active colloidal materials³¹.

In this article, we explore the effects of activity on a system of active patchy particles forming linear chains³². In section 2, we report the numerical details of the system under study: a two-dimensional suspension of active Brownian repulsive particles whose surface is decorated with two diametrically-opposed attractive sites that interact via a short-range attractive potential. In section 3, we report the results, focusing on the structural features and on two observed novel states: active spirals and spinning crystalline clusters.

2 Simulation Details and Analysis Tools

We simulate a two-dimensional system of active bivalent Brownian particles (ABBP) in a square box with periodic boundary conditions. Particles are modeled as hard-disks of diameter σ , featur-

^a Departamento de Estructura de la Materia, Física Térmica y Electrónica, Universidad Complutense de Madrid, 28040 Madrid, Spain

^b Department of Physics, Sapienza Università di Roma, Piazzale Aldo Moro 5, 00185 Rome Italy.

ing two identical and diametrically-opposed attractive sites, and self-propelling in the direction of the vector connecting the two sites (see Fig. 1a).

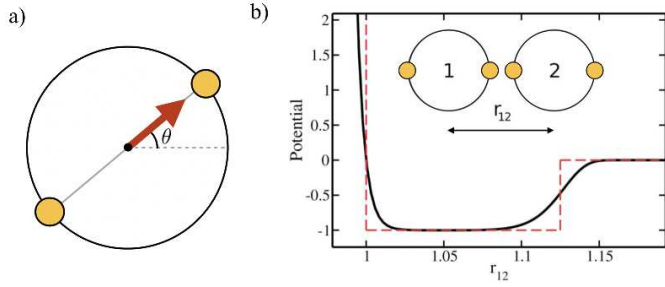


Fig. 1 a) Pictorial representation of ABBPs: hard-disks featuring two identical and diametrically-opposed attractive sites (small golden disks) and self-propulsion (red arrow) along the segment connecting the two sites. b) Interaction potential between two ABBPs in the most favorable bonding configuration, i.e., when two sites are facing each other (see inset). The dashed red line represent the hard-core plus square-well potential used as reference for the choice of the interaction potential.

The two-body interaction potential between particles i and j is given by:

$$V(i, j) = V_{CM}(i, j) + V_S(i, j) \quad (1)$$

where $V_{CM}(i, j)$ represents the hard-core interaction between the centers of mass and $V_S(i, j)$ the directional attractive interaction between the sites. Specifically, as in³³, we choose:

$$V_{CM}(i, j) = \left(\frac{\sigma}{r_{ij}} \right)^m \quad (2)$$

$$V_S(i, j) = - \sum_{a=1}^2 \sum_{b=1}^2 \varepsilon \exp \left[-\frac{1}{2} \left(\frac{r_{ij}^{ab}}{\alpha} \right)^n \right] \quad (3)$$

where r_{ij} is the distance between the centers of mass of the two particles and r_{ij}^{ab} is the distance between sites a and b located on particles i and j respectively. The selected interaction potential incorporates the following assumptions: 1) particles are hard ($m = 200$); 2) the site-site V_S interaction resembles a square-well ($n = 10$); 3) the single bond per site condition is fulfilled ($\alpha = 0.12$); 4) the potential depth u_0 is set to 1 ($\varepsilon = 1.001$). Fig. 1b depicts the shape of the interaction potential (black line) when two particles are in the most favorable bonding configuration.

Each particle is characterized by the position vector of its center of mass $\mathbf{r} = (x, y, 0)$ and the orientation angle θ representing the direction of the vector connecting the two sites with respect to the x -axis. The orientation vector $\boldsymbol{\eta} = (\cos \theta, \sin \theta, 0)$ is applied at each particle's center of mass and is restricted to rotate in the two-dimensional plane of the system.

While self-propelling in the same direction of the orientation vector with a constant speed v , each particle undergoes Brownian motion, in both position and orientation, at a constant temperature T . Thus, for a particle i , the translational and rotational equations of motion, read as:

$$\dot{\mathbf{r}}_i(t) = \frac{D_T}{K_B T} \mathbf{F}_i(\{\mathbf{r}_{ij}, \boldsymbol{\eta}_i, \boldsymbol{\eta}_j\}) + v \boldsymbol{\eta}_i(t) + \sqrt{2D_T} \boldsymbol{\xi}_T(t) \quad (4)$$

$$\dot{\boldsymbol{\eta}}_i(t) = \frac{D_R}{K_B T} \mathbf{T}_i(\{\mathbf{r}_{ij}, \boldsymbol{\eta}_i, \boldsymbol{\eta}_j\}) + \sqrt{2D_R} \boldsymbol{\xi}_R(t) \times \boldsymbol{\eta}_i(t) \quad (5)$$

The diffusion coefficients D_T and D_R relate to each other via $D_R = 3D_T/\sigma^2$. In both the translational and rotational equations, the Gaussian white-noise terms are characterized by $\langle \boldsymbol{\xi}(t) \rangle = 0$ and $\langle \boldsymbol{\xi}(t) \boldsymbol{\xi}(t') \rangle = \delta(t - t')$. The total force \mathbf{F}_i and torque \mathbf{T}_i acting on each particle are respectively given by:

$$\mathbf{F}_i(\{\mathbf{r}_{ij}, \boldsymbol{\eta}_i, \boldsymbol{\eta}_j\}) = \sum_{j \neq i} \mathbf{F}_{ij}(r_{ij}, \boldsymbol{\theta}_i, \boldsymbol{\theta}_j) = - \sum_{j \neq i} \nabla_{\mathbf{r}_{ij}} V_{ij}(r_{ij}, \boldsymbol{\theta}_i, \boldsymbol{\theta}_j) \quad (6)$$

$$\mathbf{T}_i(\{\mathbf{r}_{ij}, \boldsymbol{\eta}_i, \boldsymbol{\eta}_j\}) = \sum_{j \neq i} \mathbf{T}_{ij}(r_{ij}, \boldsymbol{\theta}_i, \boldsymbol{\theta}_j) = \sum_{j \neq i} \boldsymbol{\eta}_i \times \frac{\partial V_{ij}(r_{ij}, \boldsymbol{\theta}_i, \boldsymbol{\theta}_j)}{\partial \boldsymbol{\eta}_i} \quad (7)$$

where \mathbf{F}_{ij} and \mathbf{T}_{ij} are respectively the force and the torque between particles i and j interacting via the potential $V_{ij} = V(i, j)$ described in Eq. 1. The potential only depends on the distance between the two centers of mass r_{ij} and the orientations of both particles $\boldsymbol{\theta}_i$ and $\boldsymbol{\theta}_j$.

In this article, all results are reported in reduced units. The unit length is σ (one particle's diameter, which is set to 1) and the energy unit is u_0 (the potential depth, which is also set to 1). With $k_B = 1$, temperature is measured in units of energy. Time is in units of σ^2/D_T . All simulations are run for at least 10^8 steps with an integration time step of 10^{-6} units.

We set the number of particles to $N = 5000$ and simulate the system at four different number densities $\rho = N/A$ (with A the total area): $\rho = 0.1, 0.2, 0.3$, and 0.4 . Activity is quantified by means of the Péclet number, defined as in³⁴:

$$Pe = \frac{3v\tau_R}{\sigma} \quad (8)$$

being $\tau_R = 1/D_R$ the reorientation time. We fix the value of the rotational diffusion ($D_R = 3$) and vary the one of the propulsion speed. Specifically, the Péclet number varies among the following values: $Pe = 0, 1.66, 3.33, 5, 10$, and 20 (corresponding to speeds $v = 0, 1.66, 3.33, 5, 10$, and 20 respectively). Simulations in the passive regime ($Pe = 0$) are performed as reference. We choose to study the behaviour of the system at two temperatures: a lower one $T = 0.07$ and a higher one $T = 0.1$.

In order to study the assembly features of the suspension, we evaluate the chain length distribution ρ_{ch} and the cluster size distribution ρ_{cl} according to:

$$\rho_{ch}(l) = \left\langle \frac{N_l}{\sum_l N_l} \right\rangle \quad (9)$$

$$\rho_{cl}(s) = \left\langle \frac{N_s}{\sum_s N_s} \right\rangle \quad (10)$$

where N_l is the number of chains of length l , N_s is the number of clusters of size s , \sum_l and \sum_s run respectively over all chain lengths and all cluster sizes and $\langle \dots \rangle$ averages over steady state configurations. On the one hand, the chain length distribution relies on

an energetic criterion: two particles form a chain bond when their interaction energy is lower than -0.3 units. On the other hand, the cluster size distribution relies on a geometric criterion: two particles belong to the same cluster when the distance between their centers of mass is smaller than 1.2 units.

To describe the structural properties of the suspension, we compute the structure factor:

$$S(q) = \left\langle \frac{1}{N} \sum_{i=1}^N \sum_{j=1}^N e^{-i\mathbf{q} \cdot (\mathbf{r}_i - \mathbf{r}_j)} \right\rangle \quad (11)$$

where \mathbf{q} is the exchanged wave vector, \mathbf{r}_i is the coordinate of particle i and $\langle \dots \rangle$ averages over steady state configurations.

To analyze the bonding dynamics, we compare the orientation of the first and the second particle of each chain and assign $+1$ if the orientations are the same and -1 if they are not (i.e., we measure the scalar product between the two propulsion vectors and assign $+1$ if the product is greater than 0 or -1 if is less than 0). We repeat the same procedure for each pair of particles in the chain and then sum all values. Hence, for each chain i of length l , we obtain a value B_i ranging between $+(l-1)$ and $-(l-1)$. The upper limit $+(l-1)$ represents the case in which all particles are assembled with the same orientation and the lower limit $-(l-1)$ the case with alternating ones. We evaluate the average over all N_l chains of length l ($E_B(l)$) and the variance ($Var_B(l)$) as:

$$E_B(l) = \frac{\sum_{i=1}^{N_l} B_i}{N_l} \quad (12)$$

$$Var_B(l) = \frac{\sum_{i=1}^{N_l} B_i^2}{N_l} - E_B^2(l) \quad (13)$$

When the formed structures are more compact, we evaluate the hexagonal order parameter³⁵, whose expression, for each particle i , is given by:

$$\psi_i = \frac{1}{k} \sum_{j=1}^k e^{ik\theta_{ij}} \quad (14)$$

where the sum runs over the $k = 6$ nearest neighbors and θ_{ij} is the angle formed by the vector \mathbf{r}_{ij} and the x -axis.

In the context of the crystalline structure, predominantly characterized by straight chains, we evaluate the chain propulsion as follows. For each chain, we compare the orientation of the first particle with the orientation of each other particle and assign $+1$ if they are the same (scalar product greater than 0) or -1 if they are not (scalar product less than 0). Then, chain propulsion is obtained by summing all values.

To study the structures characterised by a spiral shape, we evaluate the turning number³⁶, which is computed as, for each chain i with length l , as:

$$\chi_i = \frac{1}{2\pi} \sum_{j=1}^{l-1} (\theta_{j+1} - \theta_j) \quad (15)$$

where θ_j is the angle indicating the orientation of the j -th particle of the chain with respect to the x -axis. The turning number quantifies the number of turns the chain makes between its two ends: $\chi_i = 0$ (straight chain) and $\chi_i = 1$ (one circle chain). In par-

ticular, we are interested in the average value over all chains of the system. We underline that one could also use the end-to-end distance of the chain to characterise the spiral state, but in the present work we will focus on the turning number.

3 Results

We start by analysing the phase behaviour of the suspension when varying activity and density. Fig. 2 reports two panels, each showing snapshots taken once the system was in steady state: the top one represents the system at a lower temperature ($T = 0.07$) and the bottom one at a higher temperature ($T = 0.1$).

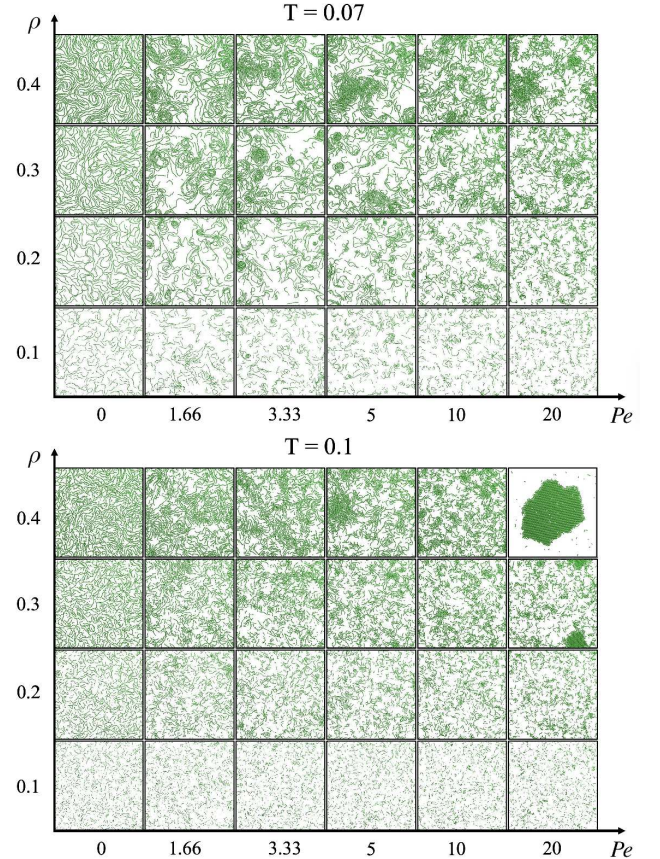


Fig. 2 Steady state configurations, as a function of activity and density, at temperature $T = 0.07$ (top panel) and $T = 0.1$ (bottom panel). Activity increases horizontally (from left to right) and density increases vertically (from bottom to top).

Passive particles (left-most column) self-assemble into uniformly space-distributed linear chains (independently of temperature and density). Increasing activity, active particles self-assemble into linear chains that aggregate with each other. These dense and compact structures are more clearly visible at the highest density (top row in both panels of Fig. 2). At the lowest temperature, aggregates appear even at lower densities (bottom rows of top panel of Fig. 2). For the largest simulated activity $Pe = 20$ (at the highest temperature, bottom panel), the system forms a compact and ordered structure.

At the lowest temperature and highest densities (rows $\rho = 0.4$ or $\rho = 0.3$ of top panel of Fig. 2), especially when activity

assumes low or mid-range values (such as $Pe = 1.66, 3.33, \text{ or } 5$), chains aggregate forming spirals which are rotating at a finite angular velocity, reminiscent of the recently experimentally observed spirals in driven actin filaments on lipid membranes³⁷. These aggregates are very different from the density fluctuations observed in the suspensions of purely repulsive active Brownian particles (MIPS)²⁴. For this reason, we define this novel state with the acronym MISp, i.e., Motility-Induced SPirals.

3.1 Chain and active spiral phase

In either passive or active systems, particles self-assemble into linear chains whose length distribution decays exponentially (see Fig. 3a). In active systems, chains tend to be shorter than in the corresponding passive system (black curve in Fig. 3a): the higher the activity, the shorter the chains (at all temperatures and densities). Therefore, activity clearly affects chain formation. Moreover, as activity increases, a consistently more pronounced peak is observed at small chain lengths, likely due to the higher diffusivity of small chains as compared to long ones.

On top of that, as density increases, chains aggregate forming clusters (see Fig. 3b). Both passive and active clusters exhibit percolation at the highest density. In fact, all cluster size distributions follow the same power law: $\rho_{cl}(s) \sim s^{-\tau}$ with $\tau = 2.05$, which is consistent within the random percolation universality class³⁸.

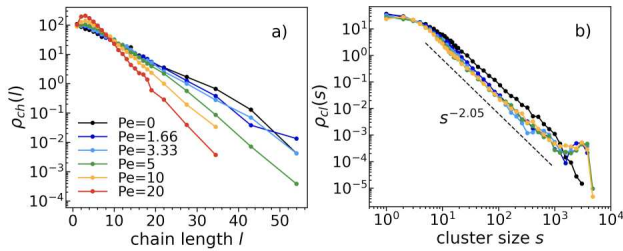


Fig. 3 a) Chain length distributions at temperature $T = 0.1$, density $\rho = 0.3$, and all studied Péclet numbers (see legend). All distributions decay exponentially, with higher decay rate at larger Péclet numbers. This observation holds also at the other studied temperature and densities. b) Cluster size distributions at temperature $T = 0.1$, density $\rho = 0.4$, and all studied Péclet numbers, except $Pe = 20$, where the system is in a crystalline phase. All distributions follow the same power law: $\rho_{cl}(s) \sim s^{-\tau}$ with $\tau = 2.05$ (percolation critical exponent in two dimensions). This observation holds also at the other studied temperature.

Even though clusters percolate in both passive and active systems, their structures differ significantly due to activity. Fig. 4 illustrates the structure factor at different Péclet numbers. As expected, due to the excluded volume effects, $S(q)$ oscillates with periodicity set by the diameter. Chaining manifests in the non-negligible values at small q . Regarding the first neighbors peak, it becomes less pronounced increasing activity, as the chaining effect is less noticeable.

An important finding in the $S(q)$ of passive systems is the presence of a peak at $q\sigma \approx 3$, which indicates alignment within chains. As activity increases, the peak shifts towards that of the first neighbors and, so, disappears. Its disappearance implies that

chains are aggregating among each other instead of being uniformly distributed, as a characteristic distance between chains is no longer evident.

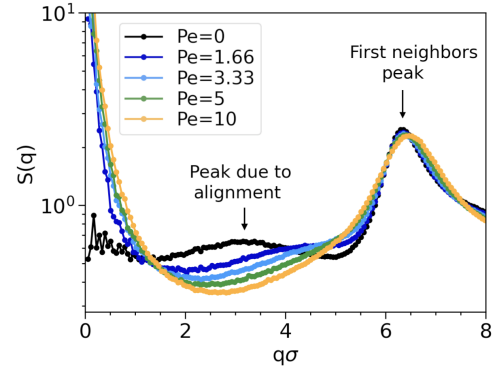


Fig. 4 Structure factors $S(q)$ at temperature $T = 0.1$, density $\rho = 0.4$, and all studied Péclet numbers, except $Pe = 20$, where the system is in a crystalline phase (see legend). The peak at $q\sigma \sim 3$, indicating chain alignment, disappears as activity increases. This observation holds also at the other studied temperature and densities.

To better understand chaining, we study the dynamics of the bonding process, to unravel whether particles have a tendency to self-assemble into chains with similar or opposite orientation and whether such tendency is related to activity. At low activities, $E_B(l) \sim 0$ and $Var_B(l) \sim l - 1$ (see Fig. 5). This means that B_i follows a Bernoulli distribution with equal probability of success (particle placed with the same orientation of the preceding one) and failure (particle placed with the opposite orientation of the preceding one). Hence, attraction dominates over activity in the bonding process, leading self-assembly to occur randomly regardless of the particle orientations.

As activity increases, Fig. 5 shows that both $E_B(l)$ and $Var_B(l)$ consistently take larger values. This indicates, for every bonding event, an increase of the probability of two particles to self-assemble with the same orientation and a decrease of the probability to self-assemble with opposite ones. In this instance, self-assembly occurs favouring an alignment of the propulsion vectors. Hence, as correlations between particle orientations emerge, high activities affect the bonding process.

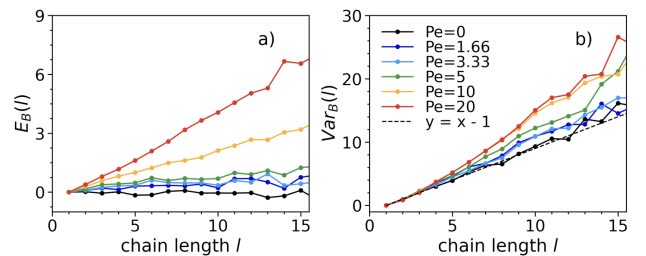


Fig. 5 $E_B(l)$ (left) and $Var_B(l)$ (right) at temperature $T = 0.1$, density $\rho = 0.3$, and all studied Péclet numbers (see legend). As activity increases, $E_B(l)$ and $Var_B(l)$ take larger value consistently. This observation holds also for the other studied temperature and densities.

At the lowest temperature and highest values of density and activity, chains aggregate forming rotating spirals. A movie rep-

representing spiral formation is shown in the Supporting material. The pathway for spiral formation is characterised by few steps: 1) ABBPs self-assemble to form long chains; 2) chains aggregate due to their persistent velocity; 3) due to combined density and temperature effects, chains merge forming spirals, that spin due to alignment within the chains.

We characterise the MISP state via the average turning number χ (being χ small when spirals are not present and large when spirals are present in the system). In particular, we compare the values of the turning number at a given Péclet number ($Pe = 1.66$) and density ($\rho = 0.4$), while varying the temperature. At the highest temperature ($T = 0.1$), $\chi = 0.13$, whereas at the lowest temperature ($T = 0.07$), $\chi = 0.40$. This confirms that the spiral structures forms at the lowest temperature. Setting the temperature at the lowest value ($T = 0.07$), spiral formation happens preferably at the higher densities, as shown in the comparison of the value $\chi = 0.21$ obtained at the lowest density ($\rho = 0.1$) and the value $\chi = 0.40$ obtained at the highest density ($\rho = 0.4$).

3.2 Spinning crystalline cluster phase

Figure 6 shows the local density distribution for the highest temperature case, evaluated performing a Voronoi tessellation of the system, at the highest temperature and density. A phase separation clearly takes place at the highest activity as shown by the rise of two distinguished peaks in the distribution (red line). Moreover, at the highest temperature, density and activity (top-right configuration of bottom panel of Fig. 2), the system forms clusters that crystallize in steady state.

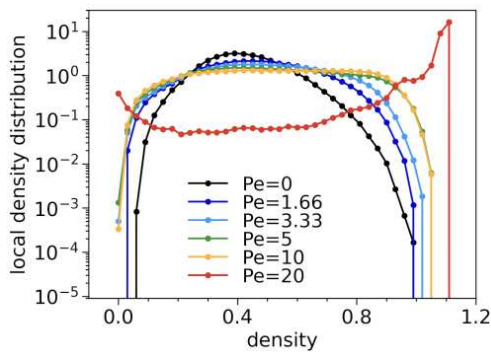


Fig. 6 Local density distribution at temperature $T = 0.1$ and density $\rho = 0.4$. A different color, according to legend, indicates a different Péclet number. At the highest Péclet number (red color), the distribution is characterized by two distinguished peaks which indicate phase separation.

Interestingly, the pathway towards crystal formation follows the steps reported in Fig. 7 (also a movie of the entire process is shown in Supporting material).

Fig. 7a) shows an initial state where chains start to form and aggregate but not in a stable way. Fig. 7b) shows a stable cluster of chains with a head (bluish chains) and a tail (yellowish chains). Yellowish chains are chains where particles are pointing all in one direction and so have a non zero chain propulsion. Fig. 7c) shows that the pushing chains in the tail allow the cluster to explore the system, leading to its growth due to the aggregation of other

rather slow chains. All chains aggregate in a compact way and activity helps to anneal defects present in the cluster increasing its crystalline order (Fig. 7d).

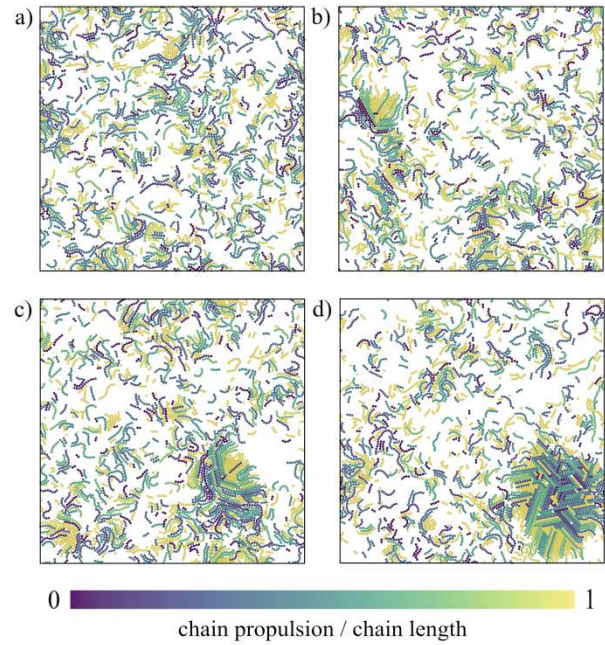


Fig. 7 Snapshots taken along the crystallization process. Particles belonging to the same chain are depicted with the same color. A different color indicates a different value of the chain propulsion (as introduced in section 2) divided by the chain length. a) Chains are forming and aggregating but there is not a stable nucleus. b) A stable nucleus is formed with a head (bluish chains) and a tail (yellowish chains). c) The nucleus is moving and aggregating chains in the head. d) The growing nucleus becomes a stable crystalline structure.

Once the crystal is formed, it is interesting to notice that it translates and rotates. To characterise its structure, we compute several properties. Fig. 8 depicts this steady state configuration in three different panels.

In Fig. 8a), particles are colored according to the value of the crystalline order parameter ψ_i (whose averaged value over all particles is $\psi \approx 0.87$). In the core of the dense structure, particles are arranged as in a hexagonal lattice with disclinations. All particles not belonging to the crystal are monomers, dimers or trimers. In Fig. 8b), particles are colored with the same color when belonging to the same chain and according to the value of the chain propulsion (as introduced in section 2) divided by the chain length. In the core of the dense structure, particles are arranged in straight chains, with alternated orientations in the innermost region and similar orientation in the outermost regions. This is due to the fact that, once the crystal core is formed, particles aggregate to it at the interface (see crystallization process in Fig. 7). In Fig. 8c), particles are colored according to the value of the orientation vector η along the x -axis. We note the presence of domains where particles are self-propelling in the same direction. The direction of such domains are indicated with black arrows. This results in an applied torque to the crystalline cluster. Thus, the crystalline cluster has a finite angular velocity other than a

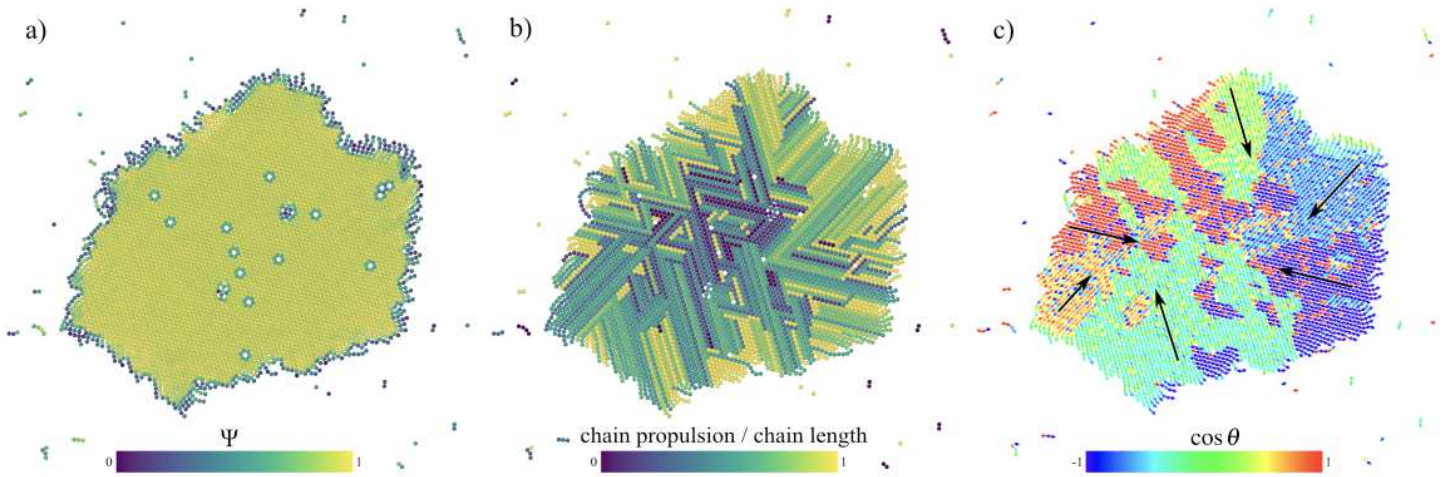


Fig. 8 Crystalline structure formed at the highest temperature ($T = 0.1$), density ($\rho = 0.4$), and Péclet number ($Pe = 20$). a) Particles are colored according to the value of the crystalline order parameter ψ_i . While $\psi_i = 1$ represents perfect order, $\psi_i = 0$ no order at all. b) Particles belonging to the same chain are depicted with the same color. A different color indicates a different value of the chain propulsion (as introduced in section 2) divided by the chain length. While 1 indicates all particles are arranged in the chain with same orientation, 0 with orientations alternated. c) Particles are colored according to the value of the orientation vector along the x -axis. Note that $\cos \theta = 1$ indicates self-propulsion toward the right side of the box, $\cos \theta = -1$ toward the left side, and $\cos \theta = 0$ toward the top or bottom side. The big black arrows indicate the main direction of self-propulsion for each domain.

translating motion of its center of mass dictated by the evaporating front.

4 Conclusion

We investigate the phase behaviour of a model system made of active Brownian particles with two opposite-located short-range attractive sites. Our work explores the role of activity, temperature and density in the process of polymerization of active patchy particles in linear chains.

Introducing activity, particles self-assemble at steady state in aggregating chains (as opposed to uniformly space-distributed chains observed in the passive corresponding systems), forming from motility-induced spirals (lowest temperature and higher densities) to crystalline clusters (highest temperature, density and activity).

To characterise the structural features of the aggregated chains, we evaluate the cluster size distributions on an energetic and geometric basis. In particular, the first method (energetic bonds) allows us to characterize the length of the chains in function of the density, temperature and, most importantly, activity. The presence of activity reduces the average chain length at every temperature and density combination. On the other hand, the second method (geometric bonds) is evaluated with the purpose to characterize the spatial chain aggregates. As a result, we observe the onset of a percolation phenomenon in a wide range of densities.

Then, we keep trying characterization the chain aggregates. This time we exploit a well-known quantity in the description of a system's structural properties, which is the structure factor. In all passive systems at the highest density, we observe the presence of an anomalous peak in the function that we attributed to the alignment of the chains. Furthermore, as activity increases, we observe that such peak shifts towards the first neighbors peak.

This can be explained by the fact that when activity is introduced in the system, chains do not uniformly distribute but aggregate, and thus we cannot identify a characteristic length anymore.

Next, the analysis proceeds by investigating the arrangement of the particles within the chains based on the direction of the propulsion vectors. Specifically, our interest focuses on understanding whether the particles were bonding with propulsion vectors in the same or opposite direction. In systems with low activity, we find the probability of bonding in the same direction to be equal to the probability of bonding in the opposite direction, i.e., the attraction being dominant over activity in the bonding process. Interestingly, as activity increases, we note the probability of bonding in the same direction increases. This result is in agreement with our predictions of a bonding process being mainly determined by activity.

To summarize, in passive systems, clusters are made of long, aligned and slow chains, while in active systems, clusters are made of short, aggregating and fast chains.

Finally, we focus on the formation and features of the crystalline structure observed at the highest values of temperature, density and Péclet number. In particular, we discover a significant rotation of the crystal cluster. The rotation arises from an effective torque generated by the presence of domains where particles are self-propelling in the same direction. What controls the nature of the fluid-to-solid transition in this active system surely deserves further investigation.

In conclusion, the presented results demonstrate the rich dynamics and emergent phenomena in active bivalent Brownian particles highlighting the potential for a deeper understanding of out-of-equilibrium systems, and for novel applications in colloidal science.

Author Contributions

Please refer to our general author guidelines for more information about authorship.

Conflicts of interest

There are no conflicts to declare.

Data Availability Statement

The data that support the findings of this study are available from the corresponding author upon reasonable request.

Acknowledgements

C.V. acknowledges fundings IHRC22/00002 and PID2022-140407NB-C21 from MINECO. J.R. and F. S. acknowledge support by ICSC – Centro Nazionale di Ricerca in High Performance Computing, Big Data and Quantum Computing, funded by European Union – NextGenerationEU. The authors thank Jose Martin Roca, Giulia Janzen and Daniel Matoz for insightful suggestions.

Notes and references

- 1 J.-P. Hansen and I. R. McDonald, *Theory of simple liquids: with applications to soft matter*, Academic press, 2013.
- 2 E. Bianchi, J. Largo, P. Tartaglia, E. Zaccarelli and F. Sciortino, *Physical Review Letters*, 2006, **97**, year.
- 3 L. Rovigatti, J. Russo and F. Romano, *European Physical Journal E*, 2018, **41**, year.
- 4 F. Sciortino, *The European Physical Journal B*, 2008, **64**, 505–509.
- 5 J. Russo, F. Leoni, F. Martelli and F. Sciortino, *Reports on Progress in Physics*, 2022, **85**, 016601.
- 6 I. Nezbeda, J. Kolafa and Y. Kalyuzhnyi, *Molecular Physics*, 1989, **68**, 143–160.
- 7 M. Ford, S. Auerbach and P. Monson, *The Journal of chemical physics*, 2004, **121**, 8415–22.
- 8 D. J. Kraft, R. Ni, F. Smalenburg, M. Hermes, K. Yoon, D. A. Weitz, A. V. Blaaderen, J. Groenewold, M. Dijkstra, W. K. Kegel, W. K. K. Designed and W. K. K. Performed, *PNAS*, 2012, **109**, 10787–10792.
- 9 R. P. Sear, *Phase behaviour of a simple model of globular proteins*, 1999.
- 10 H. Liu, S. K. Kumar and F. Sciortino, *The Journal of chemical physics*, 2007, **127**, year.
- 11 E. G. Noya, I. Kolovos, G. Doppelbauer, G. Kahl and E. Bianchi, *Soft Matter*, 2014, **10**, 8464–8474.
- 12 D. Tracey, E. Noya and J. Doye, *The Journal of Chemical Physics*, 2021, **154**, 194505.
- 13 E. Noya, C. Wong, P. Llombart and J. Doye, *Nature*, 2021, **596**, 367–371.
- 14 H. Liu, M. Matthies, J. Russo, L. Rovigatti, R. P. Narayanan, T. Diep, D. McKeen, O. Gang, N. Stephanopoulos, F. Sciortino *et al.*, *Science*, 2024, **384**, 776–781.
- 15 Y. Mai and A. Eisenberg, *Chemical Society Reviews*, 2012, **41**, year.
- 16 Y. Zhang, J. Guo, C. Zhang and K. Yang, *Advanced Materials*, 2018, **30**, year.
- 17 A. C. Mayer and G. G. Malliaras, *Advanced Materials*, 2007, **19**, year.
- 18 N. A. Kotov, *Nature*, 2001, **413**, year.
- 19 R. Mezzenga, *Current Opinion in Food Science*, 2015, **4**, year.
- 20 C. Bechinger, R. Di Leonardo, H. Löwen, C. Reichhardt, G. Volpe and G. Volpe, *Rev. Mod. Phys.*, 2016, **88**, 045006.
- 21 W. Francis G. and D. Jörn, *Nature*, 2016, **536**, year.
- 22 W. F. G. and D. J., *Nature Communications*, 2017, **8**, year.
- 23 B. M. Mognetti, A. Šarić, S. Angioletti-Uberti, A. Cacciuto, C. Valeriani and D. Frenkel, *Physical Review Letters*, 2013, **111**, year.
- 24 J. Stenhammar, R. Wittkowski, D. Marenduzzo and M. E. Cates, *Physical Review Letters*, 2015, **114**, year.
- 25 F. Alarcon, E. Navarro-Argemí, C. Valeriani and I. Pagonabarraga, *Physical Review E*, 2019, **99**, year.
- 26 S. A. Mallory and A. Cacciuto, *Journal of the American Chemical Society*, 2019.
- 27 S. A. Mallory, F. Alarcon, A. Cacciuto and C. Valeriani, *New Journal of Physics*, 2017, **19**, year.
- 28 Z. Wang, Z. Wang, J. Li, S. T. H. Cheung, C. Tian, S. H. Kim, G. R. Yi, E. Ducrot and Y. Wang, *Journal of the American Chemical Society*, 2019, **141**, 14853–14863.
- 29 Z. Wang, Z. Wang, J. Li, C. Tian and Y. Wang, *Nature Communications*, 2020, **11**, year.
- 30 Y. Wang, Y. Wang, D. R. Breed, V. N. Manoharan, L. Feng, A. D. Hollingsworth, M. Weck and D. J. Pine, *Nature*, 2012, **491**, 51–55.
- 31 Z. Zhang and S. C. Glotzer, *Nano Letters*, 2004, **4**, 1407–1413.
- 32 F. Sciortino, E. Bianchi, J. F. Douglas and P. Tartaglia, *Journal of Chemical Physics*, 2007, **126**, year.
- 33 J. Russo, P. Tartaglia and F. Sciortino, *Journal of Chemical Physics*, 2009, **131**, year.
- 34 J. Martin-Roca, R. Martinez, L. Alexander, A. Diez, D. Aarts, F. Alarcón, J. Ramirez and C. Valeriani, *The Journal of Chemical Physics*, 2021, **154**, 164901.
- 35 D. R. Nelson and B. I. Halperin, *Physical Review B*, 1979, **19**, 2457–2484.
- 36 R. E. Isele-Holder, J. Elgeti and G. Gompper, *Soft Matter*, 2015, **11**, 7181–7190.
- 37 A. Sciortino and A. R. Bausch, *Proceedings of the National Academy of Sciences*, 2021, **118**, e2017047118.
- 38 D. Stauffer and A. Aharony, *Introduction to Percolation Theory*, Taylor & Francis, London, 2nd edn, 1992.

